QKSAN: A Quantum Kernel Self-Attention Network

Ren-Xin Zhao, Member, IEEE, Jinjing Shi*, Senior Member, IEEE, and Xuelong Li, Fellow, IEEE

Abstract—Self-Attention Mechanism (SAM) is skilled at extracting important information from the interior of data to improve the computational efficiency of models. Nevertheless, many Quantum Machine Learning (QML) models lack the ability to distinguish the intrinsic connections of information like SAM, which limits their effectiveness on massive high-dimensional quantum data. To address this issue, a Quantum Kernel Self-Attention Mechanism (QKSAM) is introduced, which combines the data representation benefit of Quantum Kernel Methods (QKM) with the efficient information extraction capability of SAM. A Quantum Kernel Self-Attention Network (QKSAN) framework is built based on QKSAM, with Deferred Measurement Principle (DMP) and conditional measurement techniques, which releases half of the quantum resources with probabilistic measurements during computation. The Quantum Kernel Self-Attention Score (QKSAS) determines the measurement conditions and reflects the probabilistic nature of quantum systems. Finally, four QKSAN models are deployed on the Pennylane platform to perform binary classification on MNIST images. The best-performing among the four models is assessed for noise immunity and learning ability. Remarkably, the potential learning benefit of partial QKSAN models over classical deep learning is that they require few parameters for a high return of 98% ± 1% test and train accuracy, even with highly compressed images. QKSAN lays the foundation for future quantum computers to perform machine learning on massive amounts of data, while driving advances in areas such as quantum Natural Language Processing (NLP).

Index Terms—Machine learning, Quantum machine learning, Quantum kernel methods, Self-attention mechanism, Quantum kernel self-attention mechanism, Quantum neural network, Quantum circuit.

1 INTRODUCTION

In recent years, QML has developed tremendously [1–3]. However, many current QML models treat each quantum data equally and neglect the value of the intrinsic connections between data, which demands large amounts of expensive quantum storage to remember all the information while hampering future large-scale quantum data processing on quantum computers. If in the classical domain, the above urgent issues can be effectively addressed by SAM.

SAM was originally proposed in 2017 [4] as a module that generates new sequences by calculating self-attention scores from the sequences themselves, which allows machine learning models to better capture crucial messages in the sequences while relying less on external information, thereby dramatically boosting the processing efficiency of models. To date, SAM has accomplished impressive achievements in NLP [5, 6], computer vision [5, 7, 8], recommender system [9–11] and other fields with the above advantages. One of the prominent instances is that the application of global SAM has enabled the BoTNet model to realize 84.7% top-1 accuracy in the ImageNet benchmark test, which is unattainable before SAM is designed [12]. Albeit very powerful, the time and memory complexity of classical SAM [4] scales quadratically with sequence length, thus hampering its exploitation in domains with long contexts. A new idea for dilemma of SAM is offered by kernel methods. In 2019, a SAM based on kernel methods was first introduced, paving the way for designing attention using a larger representation space [13]. In 2021, SAM was substituted with a feature mapping that can directly approximate the softmax kernel, enabling the use of pre-trained weights in linear time models [14]. The above two cases substantiate strongly that

kernel methods not only outperform in data representation efficiency, but also surmount the high-complexity bottleneck, thereby ushering in novel directions for the SAM paradigm. The success of kernel methods in SAM naturally sparks interest in QKM.

QKM, a new variant of kernel methods, is receiving increasing attention as a bridge between quantum computing and classical machine learning theory. It can embed classical data into ansatzes that are difficult to simulate classically [15, 16]. This embedding process is equivalent to mapping the data nonlinearly into quantum Hilbert space, thus stimulating quantum advantages [17, 18]. Here, the quantum advantage refers to the performance of QKM beyond its classical counterpart, which is reflected in multiple aspects. Firstly, QKM exhibits exponential acceleration for specific problems that are classically arduous to generate correlations [19], such as encoding inductive bias [20], resulting in remarkable learning capabilities. Secondly, its exceptional universal approximation properties [21] and expressiveness [22] enable QKM-based QML models to handle a wide range of classical machine learning tasks while efficiently addressing bounded-error quantum polynomial-time problem.

The above statements prompt a natural inquiry into whether the merits of QKM and SAM can be merged to yield new models to further strengthen the data representation and information extraction capabilities of the QML framework for undifferentiated training data. The subsequent pivotal challenge is how to present the combination of QKM and SAM mechanisms in the form of quantum circuits. The last concern is how effective the framework is in practice. To this end, the **contribution** of this paper lies in addressing these pertinent inquiries and presenting novel insights into the potential of this novel QML framework: (I) From a

quantum perspective, the QKSAM theory is proposed to establish the QKM and SAM connection. (II) Led by this theory, QKSAN framework in Figure 1 is constructed for the MNIST image binary classification task based on DMP and conditional measurement techniques. (III) At last, Angle encoding Hardware-Efficient ansatz (AnHE), Amplitude encoding Hardware-Efficient ansatz (AmHE), Angle encoding QAOA ansatz (AnQAOA) and Amplitude encoding QAOA ansatz (AmQAOA) are deployed on the Pennylane platform to demonstrate that different ansatz choices can bring fundamental differences even under the same framework. Notably, even after severe compression of the images, the partial QKSAN model has the potential advantage of trading a small number of parameters for 98% \pm 1% accuracy. Moreover, the better performing AmHE model is robust for a certain probability of noise occurrence and is more resilient to quantum amplitude damping noise.

2 PRELIMINARIES

In this section, when SAM is served as a research background, QKM and DMP are elaborated based on basic theory of quantum computing, providing the necessary prerequisites for the incubation of QKSAM and QKSAN.

Self-Attention Mechanism: SAM is the investigative background of this paper, where its input and output are defined as $\mathbf{In} = [\mathbf{w}_0, \cdots, \mathbf{w}_{n-1}]^{\mathsf{T}}$ and $\mathbf{Out} = [\mathbf{new}_{-}\mathbf{w}_0, \cdots, \mathbf{new}_{-}\mathbf{w}_{n-1}]^{\mathsf{T}}$ respectively. In is computed with the three projection matrices W_Q , W_K and W_V to obtain \mathbf{Query}

$$\mathbf{Q} = \mathbf{In} \cdot W_Q = \left[\mathcal{Q}_0, \cdots, \mathcal{Q}_{n-1} \right]^{\mathrm{T}}, \tag{1}$$

Key

$$\mathbf{K} = \mathbf{In} \cdot W_K = \left[\mathcal{K}_0, \cdots, \mathcal{K}_{n-1} \right]^{\mathrm{T}}$$
 (2)

and Value

$$\mathbf{V} = \mathbf{In} \cdot W_V = \left[\mathcal{V}_0, \cdots, \mathcal{V}_{n-1} \right]^{\mathrm{T}}$$
 (3)

respectively. SAM [4] is depicted as

$$\mathbf{Out} = \mathbf{W} \times \mathbf{V},\tag{4}$$

where the self-attention score matrix

$$\mathbf{W} = \begin{bmatrix} w_{0,0} & w_{0,1} & \cdots & w_{0,n-1} \\ w_{1,0} & w_{1,1} & \cdots & w_{1,n-1} \\ \vdots & \vdots & \ddots & \vdots \\ w_{n-1,0} & w_{n-1,1} & \cdots & w_{n-1,n-1} \end{bmatrix}$$
(5)

with element

$$w_{i,j} = \operatorname{softmax}\left(\frac{\mathcal{Q}_i \mathcal{K}_j^{\mathsf{T}}}{\sqrt{d}}\right).$$
 (6)

softmax (\cdot) in Eq. (6) denotes the softmax normalization function by row. $\mathcal{Q}_i\mathcal{K}_j^{\mathsf{T}}$ indicates the inner product of matrices \mathcal{Q}_i and $\mathcal{K}_j^{\mathsf{T}}$, where $\mathcal{K}_j^{\mathsf{T}}$ is the transpose matrix of \mathcal{K}_j . \sqrt{d} is a scaling factor. With the above introduction, Eq. (6) is most prominent and represents the similarity between \mathcal{Q}_i and $\mathcal{K}_j^{\mathsf{T}}$. In Section 3, Eq. (6) is revisited through the lens of QKM to induce QKSAM.

Qubit and Quantum Gates: A figurative presentation of quantum theory can be achieved through the qubits and

quantum gates. Therein, a qubit is the smallest unit that carries information. It is usually represented by the Dirac notation

$$|\psi\rangle = \alpha|0\rangle + \beta|1\rangle,\tag{7}$$

where ground state $|0\rangle = [1,0]^T$, excited state $|1\rangle = [0,1]^T$. α and β are amplitudes satisfying $|\alpha|^2 + |\beta|^2 = 1$ [25]. As shown in Eq. (7), a qubit is in a superposition of the ground state and the excited state. This property endows it with exponential data representation abilities and a host of probabilistic features, which sets it apart significantly from classical computing. Moreover, a quantum gate can linearly transform one quantum state into another, in mathematical form as a $2^n \times 2^n$ unitary matrix, where n is the number of qubits. The quantum gates used in this paper include Hadamard gate, Pauli Y gate, Pauli Z gate, CNOT gate and Controlled Z gate as shown in supplemental material.

Quantum Kernel Methods: QKM, the first core technology of this paper, can be explained in terms of both quantum feature map and quantum overlap.

(1) Quantum feature map: The quantum gates mentioned above are employed to construct an ansatz \mathcal{U} with a fixed structure, which is tantamount to shaping a kernel function. Subsequently, the classical data are loaded into the Hilbert space via this ansatz \mathcal{U} , that is,

$$|\varphi(\mathcal{D})\rangle = \mathcal{U}(\mathcal{D})|\mathbf{0}\rangle,$$
 (8)

where $\mathcal{U}(\mathcal{D})$ denotes that the data \mathcal{D} is embedded in ansatz \mathcal{U} . The initial quantum state

$$|\mathbf{0}\rangle = |0^{\otimes n}\rangle,\tag{9}$$

where n is the number of qubits, \otimes is the tensor product notation. $\varphi(\cdot)$ is a function determined by ansatz \mathcal{U} . This process in Eq. (8) is called quantum feature map [16]. Generally, the ansatz \mathcal{U} in Eq. (8) contains entangled quantum gates like the CNOT gate, controlled Z gate, making its structure non-classical so as to provide quantum advantages. For example, a template ansatz

$$\mathcal{U}(\mathcal{D}) = \prod_{d} U(\mathcal{D}) H^{\otimes n} \tag{10}$$

is offered by Ref. [15], where d denotes the unitary operator of depth. \mathcal{D} is the data point. H are Hadamard gates.

$$U(\mathcal{D}) = \exp\left(i\sum_{S\subseteq[n]}\phi_S(\mathcal{D})\prod_{k\in S}P_i\right). \tag{11}$$

where $P_i \in \{I, X, Y, Z\}$ represents the Pauli matrices. Index $S \in \{\binom{n}{k}\}$ combinations, $k = 1, \cdots, n\}$ describes the connectivity between different qubits or data points. By default, the data mapping function

$$\phi_S(\mathcal{D}): \mathcal{D} \mapsto \left\{ \begin{array}{ll} d_i & \text{if } S = \{i\} \\ (\pi - d_i)(\pi - d_i) & \text{if } S = \{i, j\} \end{array} \right. \tag{12}$$

Furthermore, the ansatz \mathcal{U} structure can be customized to meet specific requirements.

(2) Quantum overlap: Similar to the classical kernel methods, the ultimate goal of QKM is not to obtain the way the data points are mapped but to acquire the inner product

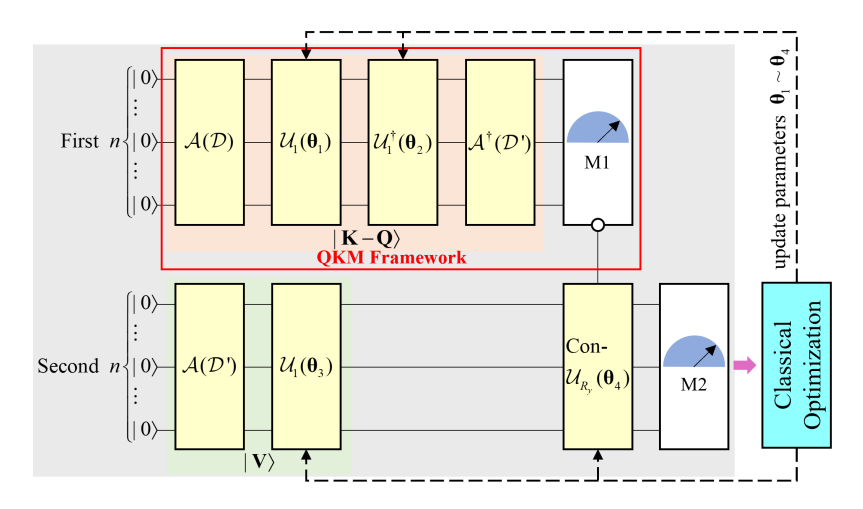
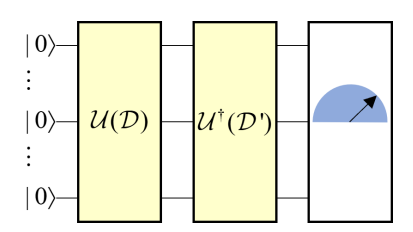


Fig. 1. Quantum kernel self-attention network framework.



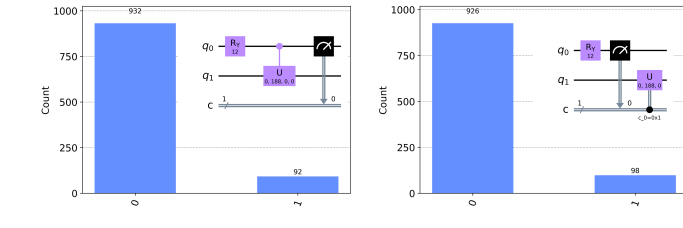


Fig. 2. Conjugate method

Fig. 3. Illustration of deferred measurement principle

between the kernel functions of two data points, which is given by the quantum overlap:

$$\kappa(\mathcal{D}, \mathcal{D}') = |\langle \varphi(\mathcal{D}) | \varphi(\mathcal{D}') \rangle|^2, \tag{13}$$

where \mathcal{D} and \mathcal{D}' in Eq. (13) represent two data points. Next, the quantum overlap $\kappa(\mathcal{D},\mathcal{D}')$ needs to be estimated using quantum circuits. Currently, there are three available options, namely conjugate method [15], Hadamard test method [26] and SWAP test method [27]. In this paper, conjugate method in Figure 2 is adopted because it eliminates ancillary qubits at the cost of circuit depth, saves quantum resources, and is relatively easy to implement compared to the Hadamard test and SWAP test. The basic principle of Figure 2 is that this circuit is initialized by state $|\mathbf{0}\rangle$ and then constructs ansatz \mathcal{U} encoded by data \mathcal{D} and conjugate transpose ansatz \mathcal{U}^{\dagger} embedded by data \mathcal{D}' . The overlap, Eq. (13), is gained by measuring the probability of observing state $|\mathbf{0}\rangle$.

Deferred Measurement Principle: The DMP [23, 24], another technical core, is a fundamental result in quantum computing that enables flexible and efficient design of quantum circuits. It asserts that postponing measurements until the end of quantum computing does not impact the probability distribution of the results, allowing measurements to be deferred to more favorable times. In particular, the DMP allows measurements to be commuted with conditional operators, providing significant freedom in designing quantum algorithms. For instance, strategically deferring measurements can reduce the number of required qubits, enable more efficient simulations. Conversely, postponing all measurements until the end of the circuit facilitates pure state analysis of the final output state, enabling the possi-

bility of more precise measurements and error correction. An example of DMP is presented in Figure 3, , illustrating that conducting measurements prior to applying conditional operators yields comparable results to direct measurements.

3 QUANTUM KERNEL SELF-ATTENTION MECHANISM

In this section, the QKSAM based on the DMP is proposed to leverage the power of QKM for elevating the data representation and information extraction capabilities of SAM while laying the foundation for QSAM research.

The first step for constructing QKSAM is to map classical data \mathcal{D} and \mathcal{D}' in \mathbf{In} to Hilbert spaces via encoding ansatz \mathcal{A} , i.e.

$$|\varphi(\mathcal{D})\rangle = \mathcal{A}(\mathcal{D})|\mathbf{0}\rangle_1$$
 (14)

and

$$|\varphi(\mathcal{D}')\rangle = \mathcal{A}(\mathcal{D}')|\mathbf{0}\rangle_2,$$
 (15)

where the subscript 1 (or 2) represents the First (or Second) register. Subsequently, a special key-query quantum state

$$|\mathbf{K} - \mathbf{Q}\rangle := \mathcal{A}^{\dagger}(\mathcal{D}')\mathcal{U}_{1}^{\dagger}(\boldsymbol{\theta}_{2})\mathcal{U}_{1}(\boldsymbol{\theta}_{1})|\varphi(\mathcal{D})\rangle$$
 (16)

is defined by applying $\mathcal{U}_1(\boldsymbol{\theta}_1)$, $\mathcal{U}_1^{\dagger}(\boldsymbol{\theta}_2)$ and $\mathcal{A}^{\dagger}(\mathcal{D}')$ sequentially to Eq. (14), where $\mathcal{U}_1^{\dagger}(\boldsymbol{\theta}_2)$ and $\mathcal{A}^{\dagger}(\mathcal{D}')$ are conjugate transpose ansatzes of $\mathcal{U}_1(\boldsymbol{\theta}_2)$ and $\mathcal{A}(\mathcal{D}')$. Using the same method for another quantum register, the value quantum state

$$|\mathbf{V}\rangle = \mathcal{U}_1(\boldsymbol{\theta}_3)|\varphi(\mathcal{D}')\rangle$$
 (17)

can also be derived. It is worth noting that the ansatzes $\mathcal{U}_1(\boldsymbol{\theta}_1)$, $\mathcal{U}_1(\boldsymbol{\theta}_2)$ and $\mathcal{U}_1(\boldsymbol{\theta}_3)$ share identical structures while

varying in parameters, which is a deliberate design choice to enforce formal equivalence of the functions.

So far, the quantum counterparts of Eq. (1) to Eq. (3), i.e. Eq. (16) and Eq. (17), have been found, but the most crucial step is still missing, namely the relationship described in Eq. (4). Observing Eq. (4) to Eq. (6), the essence of SAM lies in establishing the mathematical connection between inner product and Eq. (3), which can be equivalently understood as QKSAM constructing the connection between Eq. (16) and Eq. (17). In order to save qubits and reflect the quantum characteristics, it is not intended to construct a complex quantum multiplication network here. Instead,

QKSAS :=
$$|\langle \mathbf{0}|_1 \mathcal{A}^{\dagger}(\mathcal{D}) \mathcal{U}_1^{\dagger}(\boldsymbol{\theta}_1) \mathcal{U}_1(\boldsymbol{\theta}_2) \mathcal{A}(\mathcal{D}') |\mathbf{0}\rangle_1|^2$$
. (18)

is first acquired using mid-circuit measurements according to DMP. Then conditional operator Con- $\mathcal{U}_{R_y}(\boldsymbol{\theta}_4)$ is imposed as a mathematical relationship Θ between Eq. (16) and Eq. (17), relying on Eq. (18). Here symbol Con- $\mathcal{U}_{R_y}(\boldsymbol{\theta}_4)$ consists of Pauli Y gates, which can be involved in training to seek the best logical relationship.

Eventually, QKSAM can be described as

$$QKSAM := |\mathbf{V}\rangle\Theta_{OKSAS}.$$
 (19)

Eq. (19) implies that the relationship Θ is imposed on $|\mathbf{V}\rangle$ only when the designated ground state (e.g., $|1\rangle$ or $|0\rangle$) is measured to occur with QSKAS probability.

In summary, Eq. (19) leverages the measurement outcome of the first register to determine the application of the condition operator on Second register, consequently influencing its ansatz structure. Precisely, the conditional operator is selectively applied to the second register solely upon detection of the designated ground state, with the probability of detecting this state contingent upon the QK-SAS governed by the principle of QKM.

4 QUANTUM KERNEL SELF-ATTENTION NETWORK

In this section, the QKSAN framework is developed based on QKSAM, followed by a comprehensive explanation of the workflow and design specifics of QKSAN.

Framework of Quantum Kernel Self-Attention Network: The QKSAN framework in Figure 1 is designed as a hybrid quantum-classical architecture.

The ansatz framework of QKSAM executed on a quantum computer is depicted in the gray box. Horizontally, this ansatz framework is divided into the First and Second registers, each consisting of n qubits. Among them, the First register is inspired by the structure of Figure 2 for solving Eq. (18), where $\mathcal{A}(\mathcal{D})$, $\mathcal{U}_1(\theta_1)$, $\mathcal{U}_1^{\dagger}(\theta_2)$ and $\mathcal{A}^{\dagger}(\mathcal{D}')$ are also deployed for generating Eq. (16). The Second register is mainly employed to prepare the quantum state in Eq. (17) as well as to generate the final output M2. The control relationship Θ between the First register and the Second register is represented by the First register output M1 and ansatz Con- $\mathcal{U}_{R_y}(\theta_4)$ in Figure 1.

The components outside the gray box correspond to the classical optimization domain. A classical optimizer, such as the quantum natural simultaneous perturbation stochastic approximation optimizer [28] or the quantum natural gradient optimizer [29], is employed to update the parameters

iteratively until the loss function converges. The Nesterov momentum optimizer [30] is used in this paper, which adds a momentum term to the gradient descent that takes into account the past gradient.

Workflow for Quantum Kernel Self-Attention Network: Based on the above framework, its workflow is described here.

Step 1: The initial quantum state

$$|\Psi\rangle_1 \otimes |\Phi\rangle_2 = |\mathbf{0}\rangle_1 \otimes |\mathbf{0}\rangle_2$$
 (20)

is prepared.

Step 2: $\mathcal{A}(\mathcal{D})$, $\mathcal{U}_1(\boldsymbol{\theta}_1)$, $\mathcal{U}_1^{\dagger}(\boldsymbol{\theta}_2)$ and $\mathcal{A}^{\dagger}(\mathcal{D}')$ are applied in order for the First register while $\mathcal{A}^{\dagger}(\mathcal{D}')$ and $\mathcal{U}_1(\boldsymbol{\theta}_3)$ are used in turn for the Second one, i.e.

$$|\Psi\rangle_{1} \otimes |\Phi\rangle_{2} = (\mathcal{A}^{\dagger}(\mathcal{D}')\mathcal{U}_{1}^{\dagger}(\theta_{2})\mathcal{U}_{1}(\theta_{1})\mathcal{A}(\mathcal{D})|\mathbf{0}\rangle_{1}) \\ \otimes (I \times I \times \mathcal{U}_{1}(\theta_{3})\mathcal{A}(\mathcal{D}')|\mathbf{0}\rangle_{2})$$
(21)

where *I* is an identity matrix of size $2^n \times 2^n$.

Step 3: Conditional measurement based on DMP is performed, i.e.

$$|\Phi\rangle_{2} = \begin{cases} \operatorname{Con-}\mathcal{U}_{R_{y}}(\theta_{4})\mathcal{U}_{1}(\theta_{3})\mathcal{A}(\mathcal{D}')|\mathbf{0}\rangle_{2}, & \operatorname{P(M1)} = \operatorname{QKSAS} \\ \mathcal{U}_{1}(\theta_{3})\mathcal{A}(\mathcal{D}')|\mathbf{0}\rangle_{2}, & \text{else} \end{cases}$$
(22)

In this step, the First register undergoes measurement M1 in the middle of the circuit, resulting in the collapse of its quantum state. As a result, only the quantum state in the second register remains, effectively halving the required quantum resources. Additionally, the conditional operator $\operatorname{Con-}\mathcal{U}_{R_y}(\theta_4)$ is applied to the Second register with a probability of QKSAS.

Step 4: The expectation value

$$\mathbb{E} = \langle \Phi |_2 P | \Phi \rangle_2 \tag{23}$$

is obtained from M2, where *P* is the projection operator. Step 5: Cost function is

$$f(\mathcal{D}, \mathcal{D}', \boldsymbol{\theta}) = \frac{1}{m} \sum_{i=1}^{m} [y_i - \operatorname{sgn}(\mathbb{E})]^2,$$
 (24)

where $\operatorname{sgn}(\cdot)$ is the sign function. m is the number of terms. y_i stands for real label. The parameter θ contains θ_1 to θ_4 . The optimization rules for the Nesterov momentum optimizer are as follows:

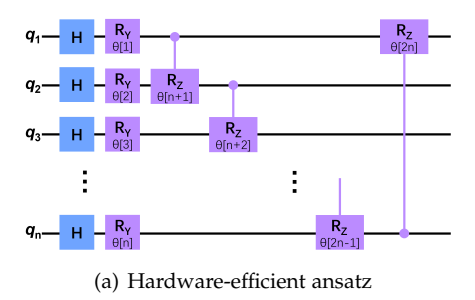
$$\begin{cases} \boldsymbol{\theta}^{(t+1)} = \boldsymbol{\theta}^{(t)} - a^{(t+1)} \\ a^{(t+1)} = \gamma \cdot a^{(t)} + \eta \cdot \nabla f(\mathcal{D}, \mathcal{D}', \boldsymbol{\theta}^{(t)} - \gamma \cdot a^{(t)}) \end{cases}$$
(25)

where the superscript t represents the t-th iteration and t+1 stands for the next iteration. The momentum term γ is adjustable and generally takes the value 0.9. η is the learning rate. $a^{(t+1)}$ and $a^{(t)}$ are accumulator terms. $\nabla f(\mathcal{D}, \mathcal{D}', \boldsymbol{\theta}^{(t)} - \gamma \cdot a^{(t)})$ denotes the gradient.

In the end, all the above steps are repeated until the cost function converge.

Ansatzes Structure: QKSAN is a generic framework, and thus its structure needs to be further refined. Specifically, the structure of two types of ansatzes (i.e., quantum encoding ansatz and trainable parameterized ansatzes) in QKSAN, is explained.

Quantum encoding ansatz A loads classical data into the Hilbert space, but its efficiently implementing remains



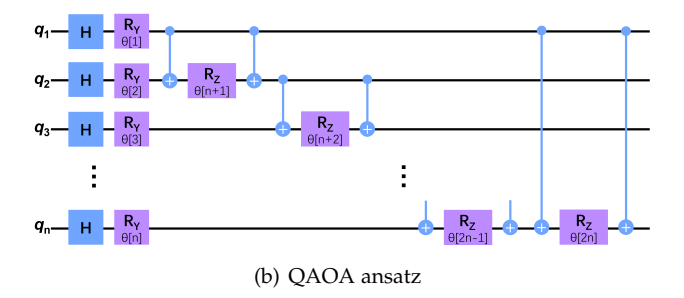


Fig. 4. Example of trainable ansatzes

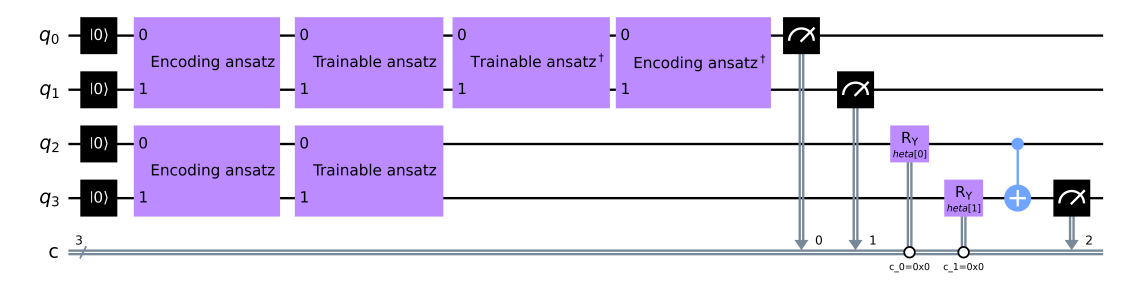


Fig. 5. Quantum kernel self-attention network framework. Encoding ansatz: angle encoding or amplitude encoding. Trainable ansatz: hardware-efficient ansatz or QAOA ansatz.

a challenge. Despite extensive efforts, the optimal encoding solution has not yet been discovered. As such, practical considerations, such as the availability of quantum resources and the simplicity of the encoding strategy, are crucial in selecting suitable encoding approaches in engineering. For example, when the number of qubits is limited, quantum amplitude encoding [31] is feasible. In spite of being timeconsuming because of the need for exponential gates to prepare quantum states, it is able to compress classical data exponentially on a quantum computer, with only t qubits required to represent 2^t classical data. In contrast, quantum angle encoding [32] is relatively simple to implement. This method directly encodes classical data into quantum gates with parameters after scaling. However, it is more susceptible to noise due to the increased number of required ansatz layers when encoding high-dimensional classical data. For additional information on encoding methods, please refer to Refs. [33, 34].

 \mathcal{U}_1 and its inverse circuit \mathcal{U}_1^\dagger as well as $\text{Con-}\mathcal{U}_{R_y}$ are ansatzes with trainable parameters, which are functionally equivalent to hidden layers in classical deep learning. The structure of \mathcal{U}_1 is set here as hardware-efficient ansatz [35, 36] in Figure 4(a) or QAOA ansatz [37, 38] in Figure 4(b) due to the mainstream influence. In fact, its architecture can also be such as random ansatz [39], MERA [40], etc. The structure of $\text{Con-}\mathcal{U}_{R_y}$ is designed for simplicity, and perhaps a more complex structure could lead to stronger learning benefits.

5 EXPERIMENT

In this section, a comprehensive assessment of the QKSAN framework for MNIST image binary classification tasks is conducted via the Pennylane platform. The experiments consist of three parts. (1) In an ideal experimental setting devoid of circuit noise and with consistent classical optimizer

settings, the performance of four specific ansatz models within the same QKSAN framework is compared. (2) To evaluate the performance of QKSAN in a real quantum computer, the effects of bit flip error and amplitude damping error on AmHE are inspected [25]. (3) A comparison with QSAN [42] is conducted to derive the advantages and limitations of QKSAN.

Models: Given the restricted availability of public quantum resources, such as the free six-qubit systems offered by IBM, Figure 5 exhibits a four-qubit QKSAN model, where q_0 to q_3 are the four qubits and c denotes the classical register used to store the measurement results. The Encoding ansatz and Trainable ansatz in this figure have two options each, with the former allowing for a choice between angle encoding or amplitude encoding ansatz, and the latter presenting the option of either hardware-efficient ansatz in Figure 4(a)or QAOA ansatz in Figure 4(b). These ansatz options are combined to form four models: AnHE, AmHE, AnQAOA and AmQAOA. It is worth noting that Figure 5 differs slightly from Figure 1. In Figure 5, an extra CNOT gate is incorporated compared to Figure 1, and the entanglement outcomes of q_3 are measured as predictive labels. In this way, these four concrete models can be used as machine learning models for MNIST data classification.

Dataset: MNIST [41] is a well-established and broadly adopted benchmark dataset in the realm of machine learning, serving as a foundation for numerous studies in the field. It consists of 10,000 test images and 60,000 training images, each containing 28×28 pixel points. For our experimentation, 550 handwritten images with label 0 and 550 handwritten images with label 1 are chosen from MNIST as the dataset. From the pool of 550 images for each label, 500 images are randomly picked as the training set, while the remaining images are served as the test set. Moreover, to cater to the aforementioned four models, the dimensionality

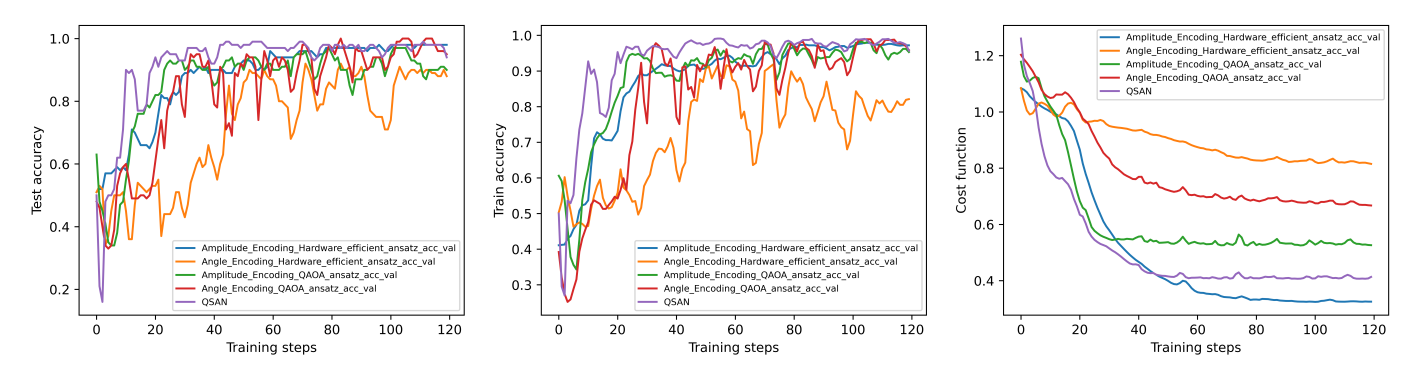


Fig. 6. Experimental results of binary classification of MNIST dataset

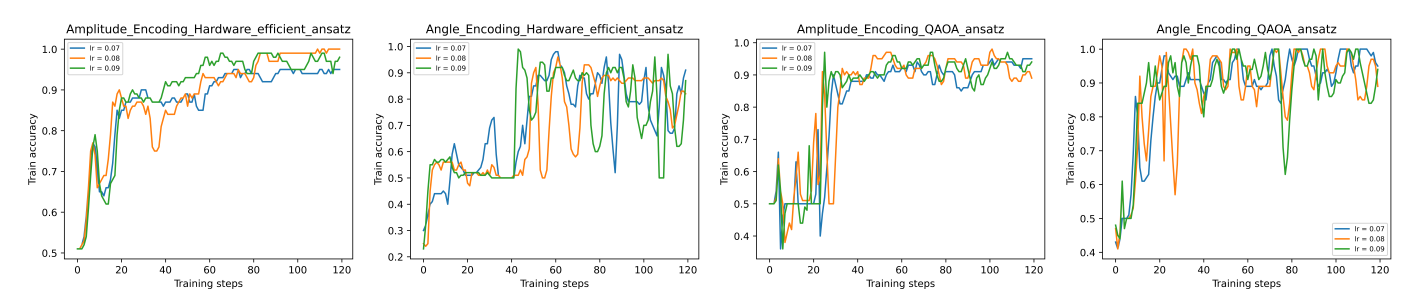


Fig. 7. Robustness to learning rate

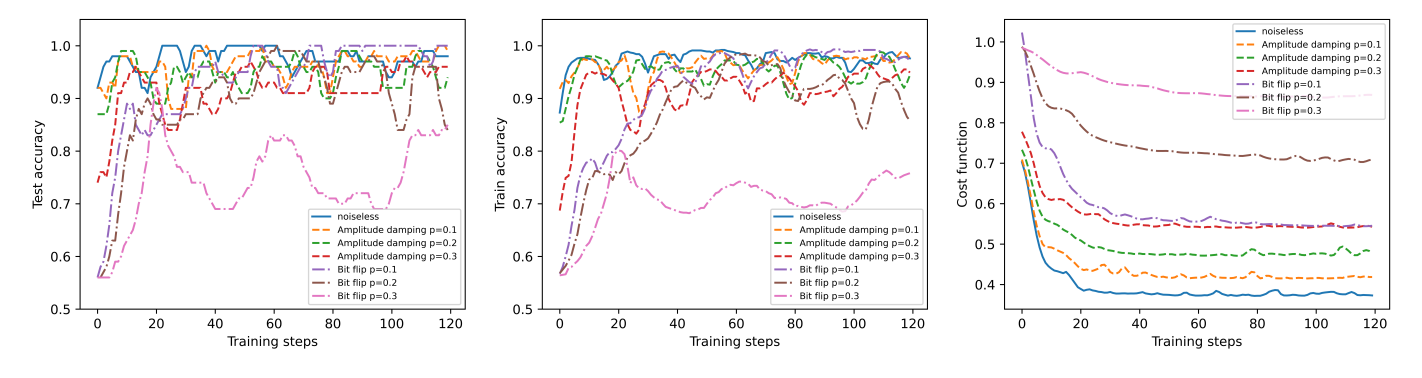


Fig. 8. Noise experiments for amplitude encoding hardware-efficient ansatz

of all images in the dataset has been compressed to 8 dimensions using the principal component analysis algorithm. Obviously, severe image compression results in the loss of a significant amount of critical information, thereby presenting challenges in image classification.

Experimental Setting: The specific experimental configuration of the QKSAN is explicated in Table 1. This table enumerates pivotal parameters of both quantum circuits and classical optimizers for AmHE, AnHE, AmQAOA, AnQAOA and QSAN [42]. As the aforementioned five models are hybrid quantum-classical frameworks, the equitable appraisal of quantum model performance is ensured and accentuated by employing classical optimizer of identical type and configuration. A larger learning rate is specifically selected for for model to expedite convergence.

Experimental Analysis: The training results and robustness to learning rate of the four models in the absence of

circuit noise are demonstrated in Figure 6 and Figure 7, respectively. Furthermore, we note that the recent research by Zhao et al. [42] bears a close connection to our own. Their scheme is implemented in Figure 6 and compared with QKSAN. Since the classical portions are identical, the differences on the quantum models radically impact the three crucial parameter metrics, namely the test accuracy, train accuracy and cost function convergence in the figure. (1) From an accuracy standpoint, AnQAOA (red line), AmHE (blue line) and QSAN (purple line) achieve an average classification accuracy of $98\% \pm 1\%$ on both the test and training sets, using 11, 15 and 9 parameters, respectively. This indicates that quantum models can trade a small number of parameters for high accuracy, which seems to be another potential advantage of QML compared to classical deep learning models. (2) The smoothness of

TABLE 1 Experimental configuration

	Models				
Indicators	AmHE	AnHE	AmQAOA	AnQAOA	QSAN [42]
parameters	11	11	15	15	9
layers	9	11	17	19	30
qubits			4		12
learning rate	0.09				
loss function	square loss				
batch_size	30				
step	120 steps				
optimizer	Nesterov Momentum Öptimizer: $\gamma=0.9$				

the blue and purple curves in relation to curve volatility implies that AmHE and QSAN exhibit greater robustness to large learning rates, whereas the other three models are more susceptible to learning rates. (3) By observing the variation of the loss function, it is evident that the five models converge to different steady-state values. The blue line shows the lowest convergence value, indicating that AmHE has stronger learning ability than the other four models. Finally, to summarize the noise-free experimental results, even if in the same framework, the quantum circuit structure profoundly affects the training effect, learning ability, and sensitivity of parameters, but it is striking that the quantum machine learning models are able to exchange a small number of parameters for high accuracy returns, which seems to be a potential learning advantage. In addition, AmHE, a subclass of QKSAN, exhibits a stronger learning capability with fewer qubits and circuit layers compared to QSAN, albeit with a slower convergence speed.

The noise experiment are depicted in Figure 8 to explore the link between the learning ability and noise immunity of AmHE. Here, the same settings as described in Table 1 is used, but with different initial parameters. The training of AmHE is then restarted to obtain the results shown in Figure 8. The results demonstrate that AmHE has less variation in learning accuracy when subjected to bit flip error and amplitude damping error with a probability of 0.1, but the learning accuracy experiences a considerable decline as the error probability increases. This reflects that AmHE has some robustness to noise. Furthermore, the AmHE loss function variations display greater resilience to amplitude damping error, resulting in a less significant decline in learning ability compared to bit flip error.

6 Conclusion

A QKSAM that integrates the advantages of both SAM and QKM is proposed to offer a larger and more complex data representation space for current QML models while extracting vital messages from quantum data with SAM. Based on QKSAM, the QKSAN framework is created using DMP and conditional measurement techniques. Specifically, four options (AmHE, AnHE, AmQAOA and AnQAOA) with identical classical configurations are available to highlight the impact of the quantum models on the results. The experimental results demonstrate that within the same QK-SAN framework, the distinct ansatz compositions of quantum models significantly impact the experimental accuracy,

learning ability, and other relevant factors. A remarkable observation is that the QKSAN model exhibits a potential learning advantage, as evidenced by the high accuracy returns of $98\% \pm 1\%$ achieved by AmHE and AnQAOA with a small number of parameters, even in the face of severe data compression of MNIST images. In the experiments involving amplitude damping and bit flip noise, AmHE demonstrates robustness within a certain range of noise interference probabilities and is particularly resilient against amplitude damping error. Our approach contributes to the QML model to pay more attention to the important parts of quantum data, laying the foundation for future quantum computers to process massive amounts of high-dimensional data.

REFERENCES

- [1] J. Shi, W. Wang et al., "Parameterized Hamiltonian learning with quantum circuit," IEEE Transactions on Pattern Analysis and Machine Intelligence, pp. 1-10, 2022.
- [2] J. Shi, Y. Tang et al., "Quantum circuit learning with parameterized Boson sampling," IEEE Transactions on Knowledge and Data Engineering, pp. 1-1, 2021.
- edge and Data Engineering, pp. 1-1, 2021.
 [3] M. Cerezo, G. Verdon et al., "Challenges and opportunities in quantum machine learning," Nature Computational Science, vol. 2, no. 9, pp. 567-576, 2022
- [4] A. Vaswani, N. Shazeer et al., "Attention is all you need," Advances in Neural Information Processing Systems, vol. 30, 2017.
- [5] H. Wang, C. Deng et al., "Asymmetric cross-guided attention network for actor and action video segmentation from natural language query," in Proceedings of the IEEE/CVF International Conference on Computer Vision, pp. 3939-3948, 2019.
- [6] J. Shi, Z. Li et al., "Two end-to-end quantum-inspired deep neural networks for text classification," IEEE Transactions on Knowledge and Data Engineering, pp. 1-1, 2021.
- [7] Y. Luo, Y. Zhang et al., "Generalizing face forgery detection with high-frequency features," in 2021 IEEE/CVF Conference on Computer Vision and Pattern Recognition (CVPR), pp. 16312-16321, 2021.
- [8] W. Xu, R. Wang et al., "MHSCNET: A multimodal hierarchical shot-aware convolutional network for video summarization," in ICASSP 2023 2023 IEEE International Conference on Acoustics, Speech and Signal Processing (ICASSP), pp. 1-5, 2023.
- [9] C. Chen, H. Geng et al., "Learning self-modulating attention in continuous time space with applications to sequential recommendation," in Proceedings of the 38th International Conference on Machine Learning, pp. 1606–1616, 2021.

- [10] Z. Chen, W. Zhang et al., "Learning dual dynamic representations on time-sliced user-item interaction graphs for sequential recommendation," in Proceedings of the 30th ACM International Conference on Information & Knowledge Management, pp. 231-240, 2021.
- [11] Q. Wu, H. Zhang et al., "Towards open-world recommendation: An inductive model-based collaborative filtering approach," in Proceedings of the 38th International Conference on Machine Learning, pp. 11329–11339, 2021.
- ference on Machine Learning, pp. 11329–11339, 2021.

 [12] A. Srinivas, T. Y. Lin et al., "Bottleneck Transformers for visual recognition," in 2021 IEEE/CVF Conference on Computer Vision and Pattern Recognition (CVPR), pp. 16514-16524, 2021.
- [13] Y.-H. H. Tsai, S. Bai et al., "Transformer dissection: An unified understanding for Transformer's attention via the lens of kernel," in Proceedings of the 2019 Conference on Empirical Methods in Natural Language Processing and the 9th International Joint Conference on Natural Language Processing (EMNLP-IJCNLP), pp. 4344-4353, 2019.
- [14] K. M. Choromanski, V. Likhosherstov et al., "Rethinking attention with performers," in International Conference on Learning Representations, 2021.
- [15] V. Havlíček, A. D. Córcoles et al., "Supervised learning with quantum-enhanced feature spaces," Nature, vol. 567, no. 7747, pp. 209-212, 2019.
- [16] M. Schuld, and N. Killoran, "Quantum machine learning in feature Hilbert spaces," Physical Review Letters, vol. 122, no. 4, pp. 040504, 2019.
- [17] M. Schuld, and N. Killoran, "Is quantum advantage the right goal for quantum machine learning?," PRX Quantum, vol. 3, no. 3, pp. 030101, 2022.[18] M. Schuld, "Supervised quantum machine learning mod-
- [18] M. Schuld, "Supervised quantum machine learning models are kernel methods," arXiv preprint arXiv:2101.11020, 2021.
- [19] Y. Liu, S. Arunachalam et al., "A rigorous and robust quantum speed-up in supervised machine learning," Nature Physics, vol. 17, no. 9, pp. 1013-1017, 2021.
- [20] J. Kübler, S. Buchholz et al., "The inductive bias of quantum kernels," Advances in Neural Information Processing Systems, vol. 34, pp. 12661-12673, 2021.
- [21] T. Goto, Q. H. Tran et al., "Universal approximation property of quantum machine learning models in quantum-enhanced feature spaces," Physical Review Letters, vol. 127, no. 9, pp. 090506, 2021.
- [22] J. Jäger, and R. V. Krems, "Universal expressiveness of variational quantum classifiers and quantum kernels for support vector machines," Nature Communications, vol. 14, no. 1, pp. 576, 2023.
- [23] Y. Gurevich, and A. Blass, "Quantum circuits with classical channels and the principle of deferred measurements," Theoretical Computer Science, vol. 920, pp. 21-32, 2022.
- [24] J. Herrmann, S. M. Llima et al., "Realizing quantum convolutional neural networks on a superconducting quantum processor to recognize quantum phases," Nature Communications, vol. 13, no. 1, pp. 4144, 2022.
- [25] M. Coggins, Introduction to quantum computing with Qiskit: Scarborough Quantum Computing Ltd, 2021.
- [26] D. Aharonov, V. Jones et al., "A polynomial quantum algorithm for approximating the jones polynomial," Algorithmica, vol. 55, no. 3, pp. 395-421, 2009.
- [27] H. Buhrman, R. Cleve et al., "Quantum fingerprinting," Physical Review Letters, vol. 87, no. 16, pp. 167902, 2001.
- [28] J. Gacon, C. Zoufal et al., "Simultaneous perturbation stochastic approximation of the quantum Fisher information," Quantum, vol. 5, pp. 567, 2021.
- [29] J. Stokes, J. Izaac et al., "Quantum natural gradient," Quantum, vol. 4, pp. 269, 2020.
- [30] Y. Nesterov, "A method for unconstrained convex minimization problem with the rate of convergence $O(1/k^2)$," in Doklady an ussr, pp. 543-547, 1983.

- [31] M. Möttönen, J. J. Vartiainen et al., "Quantum circuits for general multiqubit gates," Physical Review Letters, vol. 93, no. 13, pp. 130502, 2004.
- [32] R. Larose, and B. Coyle, "Robust data encodings for quantum classifiers," Physical Review A, vol. 102, no. 3, pp. 032420, 2020.
- [33] M. Weigold, J. Barzen et al., "Expanding data encoding patterns for quantum algorithms," in 2021 IEEE 18th International Conference on Software Architecture Companion (ICSA-C), pp. 95-101, 2021.
- [34] B. Tan, M. A. Lemonde et al., "Qubit-efficient encoding schemes for binary optimisation problems," Quantum, vol. 5, pp. 1-19, 2021.
- [35] A. Kandala, A. Mezzacapo et al., "Hardware-efficient variational quantum eigensolver for small molecules and quantum magnets," Nature, vol. 549, no. 7671, pp. 242-246, 2017.
- [36] Qiskit. "EfficientSU2," https://qiskit.org/documentation/stubs/qiskit.circuit.library.EfficientSU2.html 12 May, 2023.
- [37] E. Farĥi, J. Goldstone et al., "A quantum approximate optimization algorithm," arXiv preprint arXiv:1411.4028, 2014.
- [38] Qiskit. "Solving combinatorial optimization problems using QAOA," https://learn.qiskit.org/course/chapplications/solving-combinatorial-optimization-problems-using-qaoa 01 Sept., 2022.
- [39] J. Haferkamp, P. Faist et al., "Linear growth of quantum circuit complexity," Nature Physics, vol. 18, no. 5, pp. 528-532, 2022.
- [40] I. Cong, S. Choi et al., "Quantum convolutional neural networks," Nature Physics, vol. 15, no. 12, pp. 1273-1278, 2019.
- [41] Y. Lecun, L. Bottou et al., "Gradient-based learning applied to document recognition," Proceedings of the IEEE, vol. 86, no. 11, pp. 2278-2324, 1998.
- [42] R.-X. Zhao, J. Shi et al., "QSAN: A near-term achievable quantum self-attention network," arXiv preprint arXiv:2207.07563, 2022.